Effect of Non-linear Thermal Radiation and Radiation Absorption on Three-Dimensional Hydro-Magnetic Convective Heat and Mass Transfer Flow Over Stretching Sheet Filled with Al_2O_3-Water Based Nanofluid with Non-uniform Heat Source

Dr. Gnanaprasunamba K 1*, Dr. P. Sumathi 2

1 Assistant Professor, Department of Mathematics, S.S.A. Government First Grade College (Autonomous), Ballari, Karnataka, Email: gnanaprasuna77@gmail.com, Phone no: +91 9036124937

2 Associate Professor, Department of Mathematics, College of Agricultural engineering , Madakasira(ANGRAU) Andhra Pradesh, India, Email: p.sumathi@angrau.ac.in, Phone no : +91 8919516984

Abstract:

The influence of velocity slip, nanoparticle volume fraction parameter, chemical reaction, radiation absorption and non-linear thermal radiation on MHD three-dimensional heat and mass transfer boundary layer flow over a stretching sheet filled with *water-based* alumina nanofluid with irregular hear source is analyzed in this paper. To get more meaningful results we have taken nonlinear thermal radiation in the heat transfer process. Using similarity variables the non-linear partial differential equations converted into ordinary differential equations and are solved by using Finite-element method with quadratic shape functions. It is found that, higher the radiation absorption larger the primary velocity and smaller the secondary velocity in the flow region. The thickness of the thermal boundary layer grows and solutal boundary layer decays with increasing values of Q1. Both velocity profiles f' and g are enhanced, temperature and nanoconcentration reduces in based nanofluid as the nanoparticle volume fraction (ϕ) increase.

Keywords : Alumina-water, Nanofluid, Stretching Sheet, Radiation Absorption, Non-linear Thermal Radiation, Non-Uniform Heat Source, Finite Element Method.

Nomenclature

C_p	specific heat at constant pressure	k_s	thermal conductivity of nanoparticle
ϕ_w	uniform constant concentration	ϕ_∞	free stream concentration
K	permeability parameter	M	Magnetic parameter
Nu_x	Nusselt number	Pr	Prandtl number
Sc	Schmidt number	Sh_x	Sherwood number
q_r	radiative heat flux	T	temperature of the fluid
T_w	uniform constant temperature	T_∞	free stream temperature
v	velocity in the y - direction	w	velocity in the *z* - direction
k_0	rate of chemical reaction	u	velocity in the *x* – direction
C_{fx}	Skin-friction coefficient in *x*- direction	C_{fy}	Skin-friction coefficient in y-direction
K*	Mean absorption coefficient(x,y,*z*) Cartesian coordinates	R	Radiation parameter
θ_w	temperature parameter	U_0	suction parameter
ϕ	nanoparticle volume fraction	*a*	Stretching rate (constant)
Re_x	local Reynolds number in *x* –direction	Re_y	local Reynolds number in *y* -direction

Greek Symbols

θ	non-dimensional temperature	μ_f	dynamic viscosity of the base fluid
$(\mu)_{nf}$	dynamic viscosity of the nanofluid	η	dimensionless similarity variable
ν_f	kinematic viscosity of the base fluid	ρ_f	density of the base fluid
ρ_{nf}	density of the nanofluid	κ_f	thermal conductivity of base fluid
$(\rho c_p)_{nf}$	heat capacitance of the nanofluid	φ	non-dimensional concentration
σ	electrical conductivity	σ^*	stephan-Boltzmann constant
γ	tangential momentum coefficient	λ	molecular free path

Sub Scripts

f Base fluid, *nf* nanofluid

1. INTRODUCTION:

Due to the rapid progress in thermal engineered systems and heat exchangers, enhancement of rate of heating or co0oling has always been in demand for heating /cooling industrial processes. Poor heat transfer properties of traditional coolants have been an indispensable challenge for the scientists and engineers in heat transfer media and limit their applications. In fact the working fluids play a major contribution in the cooling systems. Recently great interest has been developed to analyse the heat transfer via nanofluids. Nanofluids are actually homogeneous mixtures of base fluids and nanoparticles with size (10-100nm) diameter. Nanofluids are considered as a promising way of enhancing the capability of heat transfer in fluids. In fact, the outstanding features of a nanofluid is its superior thermal conductivity comparing to base fluids. Nanoparticles are made from different materials, such as oxide ceramics(Al2o3,Cuo),metal nitrides (AIN, SiN),Carbide ceramics(Sic, Tic),metal s(CuAg,Au),Carbons (e.g. diamomd, graphite, carbon, nanotubes, fullerence) and functionalized nanoparticles. The term Nano was introduced by Choi [7]. Nowadays carbon nanooparticles are utilized to their higher thermal conductivity .

Buongiorno[3] has reported seven possible mechanisms associating nanofluid natural convection through moment of nanoparticles in the base fluid using scale analysis. These mechanisms are nanoparticle size, inertia, particle agglomeration, Magnus effect, volume fraction of the nanoparticle, Brownian motion, particle size, thermophoresis etc. Several authors, (Kleinstreuer and Feng [13], Liao [16], Ozerinc et.al. [21], Sudarsan Reddy and Chamkha[30,31], Sudarsana Reddy et.al.[32], Sundar et.al.[33], Chamkha e*t al.*,[4, 5], Kuznetsov and Nield [14]) have presented numerical and experimental studies to know the thermal conductivity enhancement of the nanofluids and Brownian motion and thermophoresis.

Thermal radiation plays very significant role in the surface heat transfer when convection heat transfer is very small and it has specific applications in the design of various innovative energy conversion systems working at high temperature. In view of above applications, Dulal pal *et al.*, [8] has analyzed the MHD boundary layer flow, heat and mass transfer of a fluid over a stretching sheet. Many investigators have been (Punnet Rana *et al.*, [24], Cheng [6], Behseresht *et al.*,[1], Kuznetsov *et al.*, [15], Rashidi *et al.*, [25], Sudarsana Reddy *et al.*, [29], Sreedevi *et al.*, [28], Sheremet *et al.*,[27]. Nogrehabadi *et al.* [20], Pop *et al.* [23]) reported the flow, heat and mass transfer of nanofluid over a stretching sheet. Recently, Ghalambaz *et al.*, [9], Sudarsana Reddy *et al.*, [29] have been analyzed the

influence of nanoparticle diameter and concentration on natural convection heat and mass transfer of Al_2O_3 –water, Ag – water and Cu – water based nanofluids over a vertical cone.

One of the serious issues all over the world at present is sustainable energy generation. Solar energy through minimal environmental impact thus offers a solution. Solar energy is considered a natural way of obtaining heat, water and electricity from the nature. The radiation from solar energy and the resultant solar energized resources (wind, biomass, hydroelectricity, wave power etc.) give an explanation for most of the accessible renewable energy that is present on the earth. Solar energy is regarded as one of the best resource for clear and renewable energy. Nanoparticles through scattering of the incident radiation allow higher levels of absorption within the fluid. Therefore, the utilization of nanofluids in solar thermal system seems quite interesting area of research.

Also energy equation in the present investigation is non-linear, i.e temperature function is not expanded about the ambient temperature**.** Sakiadis flow with nonlinear Rosseland thermal radiation, nonlinear radiative heat transfer in the flow of nanofluid due to solar energy have been studied by Pantokratoras and Fang [22], Mushtaq et al [18]. Shehzad et al [26], Mustafa et al [19], Hayat et al [11]. Hayat et al [12], Tasawar and Hayat et al [34], Reddy [17] have discussed nonlinear thermal radiation in three-dimensional flow of Jeffrey nanofluid. Mustafa et al [19] analysed nonlinear radiative heat transfer in the stagnation point flow of power law fluid. Recently Prabhavathi et al [23a] have discussed three-dimensional heat and mass transfer flow over a stretching sheet filled with Al_2O_3-water based nanofluid with heat generation/absorption.

In this paper, an attempt have been made to investigate the impact of variation absorption and chemical reaction on nonlinear convective heat and mass transfer flow of Al2O3-water nano fluid past stretching sheet in the presence of irregular heat sources. The transformed boundary layer equations which represent the flow, heat and mass transfer are solved numerically using finite element method with quadratic interpolation function. A velocity, temperature and nano-concentration have been depicted graphically for different parameters. The rate of heat and mass transfer on the wall have been numerically evaluated.

2. MATHEMATICAL FORMULATION

Consider the steady, three dimensional, viscous incompressible, laminar, MHD boundary layer flow of a nanofluid past a stretching sheet through nanofluid-saturated porous medium filled with water – based alumina nanofluid situated at $z = 0$. The coordinate system is chosen such that (u, v, w) be the velocity components along (x,y,z) directions respectively. We also consider a constant magnetic field of strength B_0 in the z - direction. The flow is caused by the stretching of the sheet which moves in its own plane with the surface velocity ax, where a (stretching rate) is positive constant. The stretching surface is maintained at uniform temperature and concentration T_w and ϕ_w and these values are assumed to be greater than the ambient temperature and concentration T_∞ and ϕ_∞ respectively. Under the above assumptions, the governing equations describing the momentum, energy and concentration in the presence of thermal radiation, chemical reaction, take the following form:

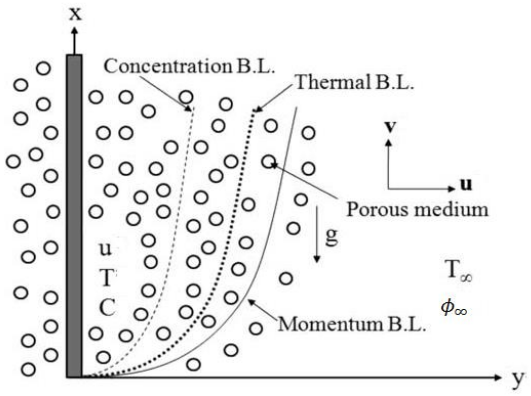

Fig. 6.1 Physical model and Coordinate system

$$\frac{\partial u}{\partial x}+\frac{\partial v}{\partial y}+\frac{\partial w}{\partial z}=0 \tag{1}$$

$$u\frac{\partial u}{\partial x}+v\frac{\partial u}{\partial y}|+w\frac{\partial u}{\partial z}=\frac{\mu_{nf}}{\rho_{nf}}\frac{\partial^2 u}{\partial z^2}-\frac{\mu_{nf}}{\rho_{nf}}\frac{1}{k}u-\frac{1}{\rho_{nf}}\sigma_{nf}B_o^2u+(\rho\beta)_{nf}(T-T_\infty) \tag{2}$$

$$u\frac{\partial v}{\partial x}+v\frac{\partial v}{\partial y}|+w\frac{\partial v}{\partial z}=\frac{\mu_{nf}}{\rho_{nf}}\frac{\partial^2 v}{\partial z^2}-\frac{\mu_{nf}}{\rho_{nf}}\frac{1}{k}v-\frac{1}{\rho_{nf}}\sigma_{nf}B_o^2v \tag{3}$$

$$u\frac{\partial T}{\partial x}+v\frac{\partial T}{\partial y}|+w\frac{\partial T}{\partial z}=\alpha_{nf}\frac{\partial^2 T}{\partial z^2}-\frac{1}{(\rho C_p)_{nf}}\frac{\partial q_z}{\partial z}+\frac{1}{(\rho C_p)_{nf}}q'''+\frac{Q_1^{'}}{(\rho C_p)_{nf}}(C-C_\infty) \tag{4}$$

$$u\frac{\partial C'}{\partial x}+v\frac{\partial C'}{\partial y}|+w\frac{\partial C'}{\partial z}=D_B\frac{\partial^2 C'}{\partial z^2}+\frac{D_TK_T}{T_\infty}\frac{\partial^2 T}{\partial z^2}-k_c(C-C_\infty) \tag{5}$$

The associated boundary conditions are

$$u=ax+\frac{2-\lambda}{\lambda},v=by+\frac{2-\lambda}{\lambda}\delta\frac{\partial v}{\partial z},w=-U_o,T=T_wC=C_w \quad at\ z=0$$
$$u\to\infty,v\to 0,T\to T_\infty,C'\to C_\infty \quad as\ z\to\infty \tag{6}$$

The dynamic viscosity μ_{nf} , density, ρ_{nf} thermal diffusivity α_{nf} , thermal conductivity $(\rho C_p)_{nf}$ specific heat , k_{nf} heat capacitance , electric conductivity σ_{nf} of the nanofluid and kinematic viscosity ν_f of the base fluid are defined as follows:

$$\alpha_{nf}=\frac{k_{nf}}{(\rho C_p)_{nf}},\mu_{nf}=\frac{\mu_f}{(1-\phi)}\ \nu_f=\frac{\mu_f}{\rho_f},\rho_{nf}=(1-\phi)\rho_f+\phi\rho_s$$
$$(\rho C_p)_{nf}=(1-\phi)(\rho C_p)_f+\phi)(\rho C_p)_s,(\rho\beta)_{nf}=(1-\varphi)(\rho\beta)_f+\varphi(\rho\beta)_s$$
$$\sigma_{nf}=\sigma_f(1+\frac{3(\sigma-1)\phi}{\sigma+2-(\sigma-1)\phi}),\sigma=\frac{\sigma_s}{\sigma_f},k_{nf}=k_f(\frac{k_s+2k_f-2\phi(k_f-k_s)}{k_s+2k_f+2\phi(k_f-k_s)}) \tag{7}$$

The similarity transformations are introduced as

$$\eta=(\sqrt{\frac{a}{\nu_f}})y,u=axf'(\eta),v=byg'(\eta),w=-(\sqrt{(a\nu_f)})(f+g),$$
$$\theta=\frac{T-T_\infty}{T_w-T_\infty},C=\frac{C'-C_\infty}{C_w-C_\infty} \tag{8}$$

By using Rosseland approximation for radiation, the radiative heat flux q_r is defined as

$$q_r = -\frac{4\sigma^* T_\infty^3}{3\beta_R}\frac{\partial T'^4}{\partial z} = -\frac{16\sigma^* T_\infty^3}{3\beta_R}\frac{\partial^2 T}{\partial z^2} \tag{9}$$

The non-dimensional temperature $\theta = \frac{T - T_\infty}{T_w - T_\infty}$ can be simplified as

$$T = T_\infty(1 + (\theta_w - 1)\theta) \tag{10}$$

where $\theta_w = \frac{T_w}{T_\infty}$ is the temperature parameter.

The non-uniform heat source/sink, q''' , is defined as

$$q''' = \frac{k_f}{x\nu_f[A_{11}(T_w - T_\infty)f' + B_1(T - T_\infty)]} \tag{11}$$

Where A_{11} and B_1 are the coefficients of space and temperature-dependent heat source/sink, respectively. The case $B_1>0$ corresponds to internal heat source and the case $B_1<0$ corresponds to internal heat sink.

Using Eqns. (8), (9) and (10), the governing non-linear partial differential equations (1) - (5) together with the boundary conditions (6) takes the form

$$f''' + A_1[(f+g)f'' - (f')^2] - Kf' - \frac{A_1A_7}{A_2}M^2 f' + (\frac{GA_1A_8}{A_2})\theta = 0 \tag{12}$$

$$g''' + A_1[(f+g)g'' - (g')^{2]} + Kg' - \frac{A_1A_7}{A_2}M^2 g' = 0 \tag{13}$$

$$\left.\begin{aligned}&(1+\frac{4Rd}{3A_4})\theta'' + \Pr\frac{A_3}{A_4}(f+g)\theta' + \frac{Rd}{A_4}(\theta_w-1)^3(3\theta^2(\theta')^2 + \theta^3\theta'') + \frac{3Rd}{A_4}((\theta_w-1)^2\\ &(2\theta^2(\theta')^2 + \theta^2\theta'') + \frac{3Rd}{A_4}((\theta_w-1)(2\theta^2(\theta')^2 + \theta^2\theta'') + \frac{1}{A_4}(A_5 f + A_6\theta) + \frac{1}{A_4}Q_1C = 0\end{aligned}\right|$$

$$C'' + Sc(f+g)C' - Sc\gamma C + ScSo\,\theta'' = 0$$

The transformed boundary conditions are

$$\begin{aligned}&f'(0) = 1 + Bf''(0), g'(0) = \alpha + Rg'(0), f(0) + g(0) = V_0,\\ &\theta(0) = 1, C(0) = 1 \qquad at\ \ \eta = 0\\ &f' = 0, g' = 0, \theta = 0, C = 0 \qquad as\ \ \eta \to \infty\end{aligned} \tag{16}$$

where, prime indicates ordinary differentiation with respect to η. In usual notations,

$$\Pr = \frac{\nu_f}{\alpha_f}.M^2 = \frac{\sigma B_o^2}{\rho_f}, K = \frac{\nu_f}{k\alpha}, Sc = \frac{\nu_f}{D_B}, Rd = \frac{4\sigma^\bullet T_\infty^3}{\beta_R k_f}, \alpha = \frac{b}{a}, B = \frac{2-\lambda}{\lambda}(\sqrt{\frac{2}{\nu_f}})\lambda_1,$$

$$\gamma = \frac{k_c}{\alpha}, A_5 = \frac{A_{11}}{a\chi}, A_6 = \frac{B_1}{ax}, A_1 = (1-\phi)^{2.5}, A_2 = 1-\phi+\phi(\frac{\rho_s}{\pi_f}),$$

$$A_3 = 1-\phi+\phi(\frac{(\rho C_p)_s}{(\rho C_p)_f}), A_4 = \frac{k_{nf}}{k_f}, A_7 = \frac{\sigma_{nf}}{\sigma_f} = 1 + \frac{3(\sigma-1)\phi}{(\sigma+2)-\phi(\sigma+1)}, A_8 = 1-\phi+\phi(\frac{(\rho\beta)_s}{(\rho\beta)_f})$$

Quantities of practical interest in this problem are the local skin-friction coefficient along *x* and *y* directions, local Nusselt number and local Sherwood number. These are defined, respectively, as

$$C_{f_x} = \frac{f''(0)}{(1-\phi)^{2.5}\,\mathrm{Re}_x^{1/2}},\ C_{fy} = \frac{g''(0)}{(1-\phi)^{2.5}\,\mathrm{Re}_x^{1/2}},\ Nu_x = -(1+R\theta_w)^2\theta'(0)\,\mathrm{Re}_x^{1/2},\ Sh_x = -C'(0)\,\mathrm{Re}_x^{1/2}$$

Table 1. Thermo - physical properties of water and nanoparticles.

Fluid	$\rho\left(\frac{Kg}{m^3}\right)$	$C_p\left(\frac{J}{kgK}\right)$	$k\left(\frac{W}{mK}\right)$	$\beta \times 10^5(K^{-1})$
Pure water	997.1	4179	0.613	21
Copper(Cu)	8933	385	401	1.67
Silver(Ag)	10500	235	429	1.89
Alumina (Al_2O_3)	3970	765	40	0.85
Titanium Oxide (TiO_2)	4250	686.2	8.9538	0.9

3. FINITE ELEMENT ANALYSIS:

The finite element analysis with quadratic polynomial approximation functions is carried out along the radial distance across the circular duct. The behavior of the velocity, temperature and concentration profiles has been discussed computationally for different variations in governing parameters. The Galarkin method has been adopted in the variational formulation in each element to obtain the global coupled matrices for the velocity , temperature and concentration in course of the finite element analysis.

Choose an arbitrary element fk and let fk, gk, θk and ϕk be the values of f, g, θ and ϕ in the element ek

We define the error residuals as

$$E_f^k = f''' + A_1[(f+g)f'' - (f')^2] - Kf' - \frac{A_1A_7}{A_2}M^2f' + (\frac{GA_1A_8}{A_2})\theta \qquad (17)$$

$$E_g^k = g''' + A_1[(f+g)g'' - (g')^{2]} + Kg' - \frac{A_1A_7}{A_2}M^2g' \qquad (18)$$

$$E_\theta^k = (1+\frac{4Rd}{3A_4})\theta'' + \Pr\frac{A_3}{A_4}(f+g)\theta' + \frac{Rd}{A_4}(\theta_w-1)^3(3\theta^2(\theta')^2+\theta^3\theta'') + \frac{3Rd}{A_4}((\theta_w-1)^2(2\theta^2(\theta')^2+\theta^2\theta'') +$$
$$+\frac{3Rd}{A_4}((\theta_w-1)(2\theta^2(\theta')^2+\theta^2\theta'') + \frac{1}{A_3}(A_5f^k + A_6\theta^k) + \frac{1}{A_4}Q_1C^k \qquad (19)$$

$$E_c^k = C'' + Sc(f+g)C' - Sc\gamma C^k + ScSo\theta'' \qquad (20)$$

where f^k, g^k θ^k & C^k are values of f, g, θ & C in the arbitrary element ek. These are expressed as linear combinations in terms of respective local nodal values.

$$f^k = f_1^k\psi_1^k + f_2^k\psi_1^k + f_3^k\psi_3^k,\ g^k = g_1^k\psi_1^k + g_2^k\psi_1^k + g_3^k\psi_3^k,\ \theta^k = \theta_1^k\psi_1^k + \theta_2^k\psi_2^k + \theta_3^k\psi_3^k,$$
$$C^i = C_1^k\psi_1^k + C_2^k\psi_2^k + C_3^k\psi_3^k$$

where ψ_1^k, ψ_2^k --------- etc are Lagrange's quadratic polynomials.

Galerkin's method is used to convert the partial differential Eqs. (18) – (20) into matrix form of equations which results into 3x3 local stiffness matrices. All these local matrices are assembled into a global matrix by substituting the global nodal values of order 1 and using inter element continuity and equilibrium conditions. . In solving these global

matrices an iteration procedure has been adopted to include the effects of pertinent parametric variations. The iteration process is continued until the desired convergence is gained.

Table 2. Comparison of $-\theta'(0)$ with previously published data.(Q1=0,A=θw=1,A5=-A6=0)

Parameter			$-\theta'(0)$	
M	θ_w	R	Hayat et al. [10]	Present Study
0.1	1.1	0.1	0.74084	0.74078
0.3	1.1	0.1	0.70977	0.70979
0.5	1.1	0.1	0.68279	0.68280
0.1	1.2	0.1	0.74410	0.74412
0.1	1.3	0.1	0.74775	0.74774
0.1	1.4	0.1	0.75180	0.75179
0.1	1.1	0.05	0.73328	0.73326
0.1	1.1	0.15	0.74802	0.74804
0.1	1.1	0.2	0.75482	0.75481

4. RESULTS AND DISCUSSION

Comprehensive numerical computations are conducted for different values of the parameters that describe the flow characteristics and the results are illustrated graphically. A representative set of computational results are presented in Figs. 2a-17d. The thermo-physical properties of water and nanoparticles are shown in Table 3. The Comparison of present results with the results reported by Hayat *et al.* [10] is made and found good agreement which is shown in Table 2.

Figs2a-d exhibit the variation of f,g,θ and C with Grashof number(G).An increase in G enhances the primary velocity and reduces the secondary velocity in the flow region. The temperature and concentration depreciate with increasing values of G. This is due to the fact that increase in G decays the t6hickness of the thermal and solutal boundaries.

It is noticed that the velocity profiles f ′ and g are both decreases as the values of M increases in the boundary layer regime. This is due to the fact that the presence of magnetic field in the flow creates a force known as the Lorentz force which acts as a retarding force as a result the momentum boundary layer thickness decelerates through out the flow region (Figs. 3a&b). Both the temperature and concentration sketches elevate as the values of magnetic parameter increases (Fig. 3c&d). This is because of the fact that, to overcome the drag force imposed by the Lorentzian retardation the fluid has to perform extra work; this supplementary work can be converted into thermal energy which increases the thickness of the thermal boundary layer.

Figs.4a-d represent f′,g,θ and C with porous parameter (K) .From the profiles we find that lesser the permeability of the porous medium smaller the velocities in the flow region. The temperature and concentration rises with increasing values of K (figs.4c&d).This may be due to the fact that increase in K leads to thickening of thermal and solutal boundary layers.

As the values of radiation parameter (Rd) raises, velocity profiles f′ reduces and g increases in based nanofluid region and is shown in Fig. 5a&b. It is perceived from Fig.5c

that as the values of θ increases the temperature profiles are also elevated This is because of the fact that the mean absorption coefficient decreases with increasing values of radiation parameter; as a result the thermal boundary layer thickness of the fluid is rises.

The variation of f ′,g,θ and C with Schmidt number(Sc) is shown in figs.6a-d.Lesser the molecular diffusivity smaller the primary velocity and larger the secondary velocity in the flow region. The thermal and solutal boundary layer thickness are educes with rising values of Sc.

The variation of f ′,g,θ and C with radiation absorption parameter(Q1) is shown in figs.7a-d. Higher the radiation absorption larger the primary velocity and smaller the secondary velocity in the flow region.The thickness of the thermal boundary layer grows and solutal boundary layer decays with increasing values of Q1(figs.7c&d).

The effect of chemical reaction (γ) on f ′,g,θ and C is exhibited in figs.8a-d.The primary velocity reduces and secondary velocity enhancers in degenerating chemical reaction case. thermal and solutal boundary layers thickness decay as the values of chemical reaction parameter (γ) rises and is shown in Fig. 8c&d..

The effect of thermo-diffusion(So)on the flow characteristics is shown in figs.9a-9d.From the profiles we notice that higher the thermo-diffusion effects larger the primary velocity and smaller the secondary velocity in the flow region.The thickness of the thermal and solutal boundary layers are reduced by increasing the values of So.

The velocity and temperature sketches of the based nanofluid for different values of space – dependent f' and temperature – dependent parameters(A_5,A_6) are depicted in Figs.10a&b to 11a&b. With higher values of f' and g the primary velocity elevates with easing values of A_5&A_6 and secondary velocity distribution diminish in the fluid region. It is observed that temperature in the thermal boundary layer increases with increase in the strength of the space depende4nt heat sink $A_5 < 0$ and reduces with that of heat source A5>0 (positive values), whereas the thermal boundary layer thickness decelerates with the decrease in the heat absorption parameters A6<0 and grows with A6>0 (positive values).This is due to the fact that the presence of the heat generating source generates the thermal energy while heat is absorbed due the presence of heat absorption source .

Figs.12a-c depict the velocity profiles along (x,y) directions for different values of nanoparticle volume fraction (ϕ).It is perceived from Fig. 12a.that both velocity profiles f' and g are enhanced in based nanofluid as the nanoparticle volume fraction (ϕ) increases. This is due to the fact that increasing the nanoparticle volume fraction enhances the momentum boundary layer thickness in the flow regime. It is noticed from Fig. 12c that the temperature profiles retards as the nanoparticle volume fraction increases. It is noticed from Fig. 12d that the concentration profiles decelerates with the increasing values of nanoparticle volume fraction (ϕ) in the based nanofluid.

It is observed from Fig.14a&b that as the values of suction parameter(fw) increases the both velocity profiles f' and g are decelerates in based nanofluid region. This is due to the fact that suction is taken away the warm fluid from the surface of the sheet and thereby decreases the thickness of the velocity boundary layer. It is seen from Figs. 14c&d that the thickness of both thermal and solutal boundary layer decays with higher values of .

It is observed from Fig. 15a&b that as the values of velocity ratio parameter (B)increases the velocity profiles of f' elevates and graphs of g are decelerates in based nanofluid region. It is seen from Figs. 15c&d that the thickness of both thermal and solutal boundary layers grows with higher values of (B).

The velocity profiles of f ′ are reduced and that of g in based nanofluid are elevated as the values of velocity slip parameter (R) increases in the boundary layer regime as shown in Fig. 16a&b.However, the thermal boundary layer thickness, as well as, solutal boundary layer thickness of based nanofluidis decays as the values of(R) rises and is shown in Fig. 16c&d.

As the values of Prandtl number (Pr) raises, both velocity profiles decreases f ′ and g accelerates in based nanofluid region and is shown in Fig. 17a&b. Furthermore, the thermal boundary layer thickness deteriorates and that of solutal boundary layer grows with higher values of Pr as shown in Fig.17c&d.

Table.3 exhibits the variation of skin friction, Nusselt and Sherwood number on $\eta=0$ for different parametric variations. An increase in Grashof number reduces the skin friction coefficient τx, enhances τz,Nu and Sh on the wall.Higher Lorentz force/ lesser the `porous permeability smaller τx,Sh and larger τz,Nu on $\eta=0$.Higher radiative heat flux/thermo-diffusion effect, larger the skin friction coefficients, smaller Nusselt and Sherwood numbers on the wall. An increase in Schmidt number(Sc) or chemical reaction parameter(γ) smaller $\tau x,\tau z$ and larger Nu,Sh on the wall. Higher radiation absorption(Q1)/ temperature ratio($A=\theta w$) larger $\tau x,\tau z$,Sh and smaller Nu, An increase in space dependent heat source(A5)/ temperature dependent heat source(A6) larger $\tau x,\tau z$, Sh while Nu reduces with A5 and enhances with A6 on $\eta=0$.An increase in nanoparticle volume fraction(ϕ) reduces $\tau x,\tau z$ and enhances Nu,Sh on the wall.An increase in B reduces $\tau x,\tau z$, Nu,Sh while τz ,Nu,Sh increases, τx reduces with increase in R. τx, reduces, τz,Nu Sh enhance with increase in suction parameter($fw>0$),The variation of $\tau x,\tau z$,Nu and Sh with Prandtl number(Pr) shows that lesser the thermal diffusivity smaller the skin friction components, Sherwood number and larger the Nusselt number on the wall.

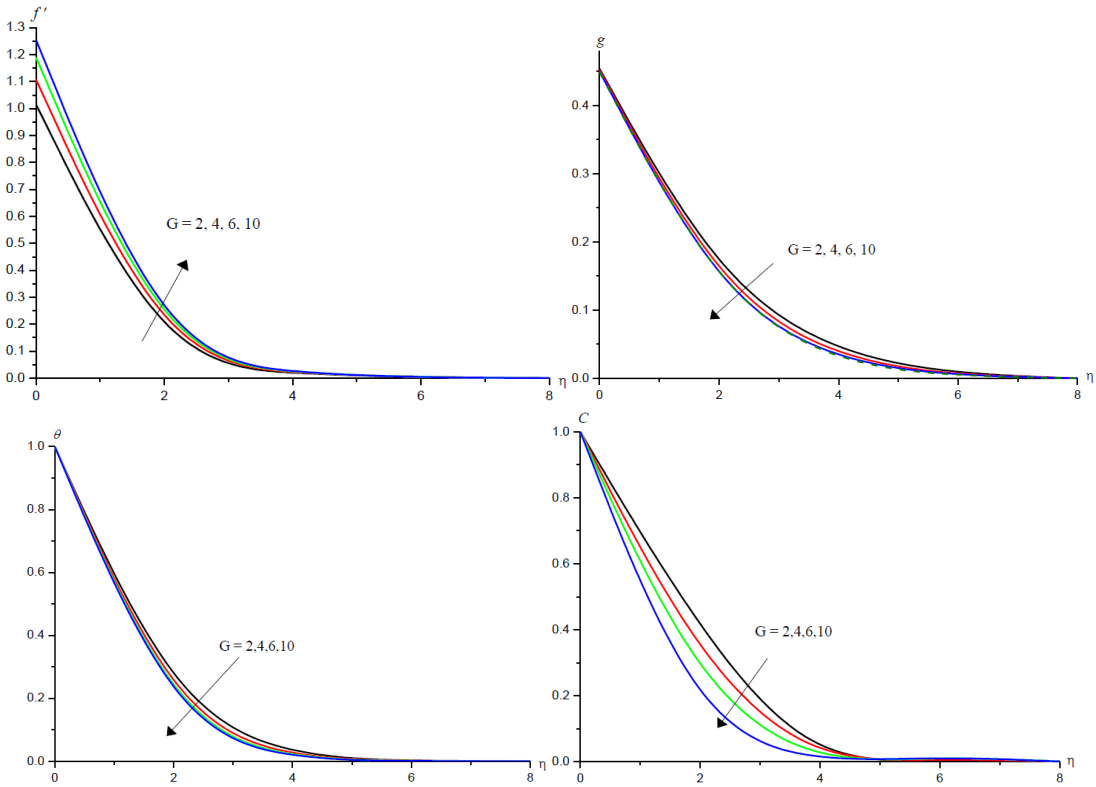

Fig.2: Variation of [a]axial velocity(f'), [b]secondary velocity(g), [c]Temperature(θ), [d]nanoconcentration(C) with G

M=0.5,K=0.2,Rd=0.5,Sc=0.66,γ=0.5,So=0.5,Q1=0.5,

A5=0.5,A6=0.6,A=1.05, ϕ=0.05,fw=0.2,B=0.2,R=0.2,Pr=6.2

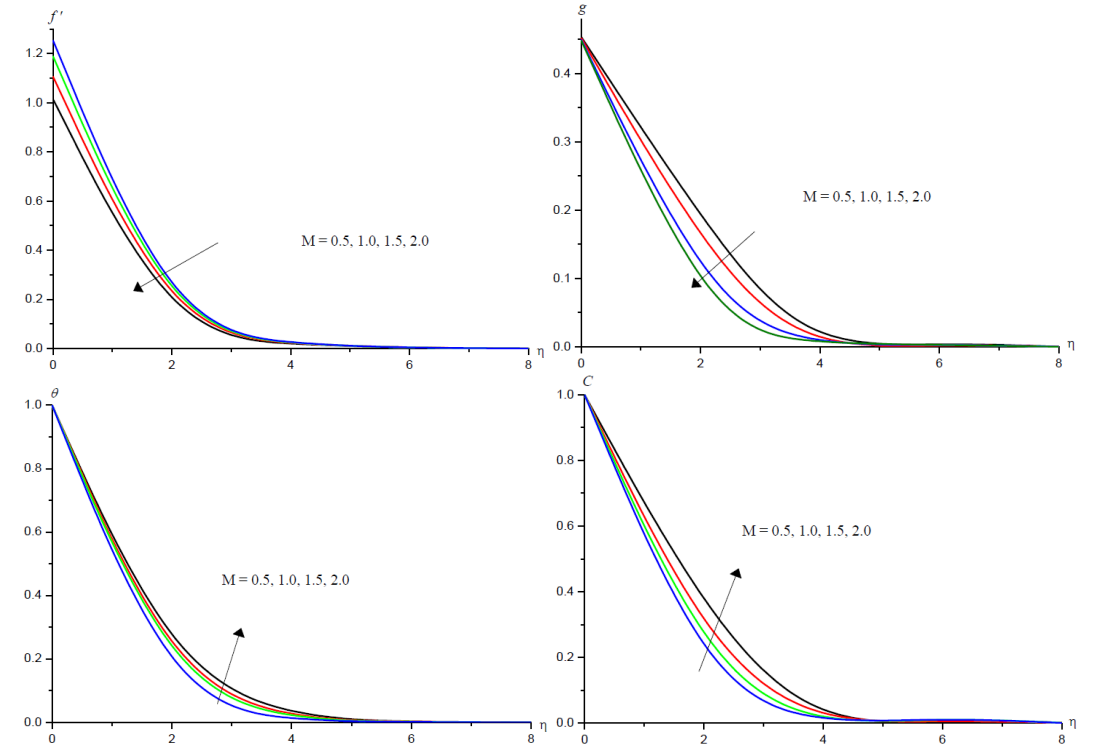

Fig.3: Variation of [a]axial velocity(f'), [b]secondary velocity(g), [c]Temperature(θ), [d]nanoconcentration(C) with M

G=2,K=0.2,Rd=0.5,Sc=0.66,γ=0.5,So=0.5,Q1=0.5,

A5=0.5,A6=0.6,A=1.05,ϕ=0.05,fw=0.2,B=0.2,R=0.2,Pr=6.2

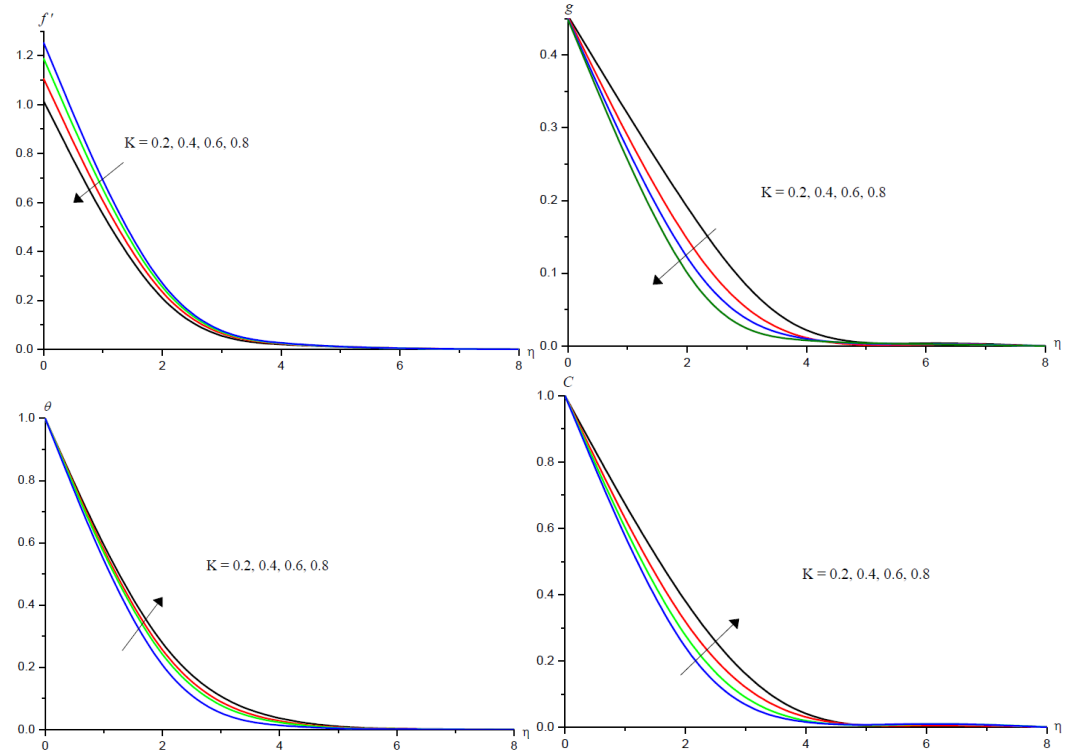

Fig.4: Variation of [a]axial velocity(f'), [b]secondary velocity(g), [c]Temperature(θ), [d]nanoconcentration(C) with K

G=2,M=0.5,Rd=0.5,Sc=0.66,γ=0.5,So=0.5,Q1=0.5,
A5=0.5,A6=0.6,A=1.05,ϕ=0.05,fw=0.2,B=0.2,R=0.2,Pr=6.2

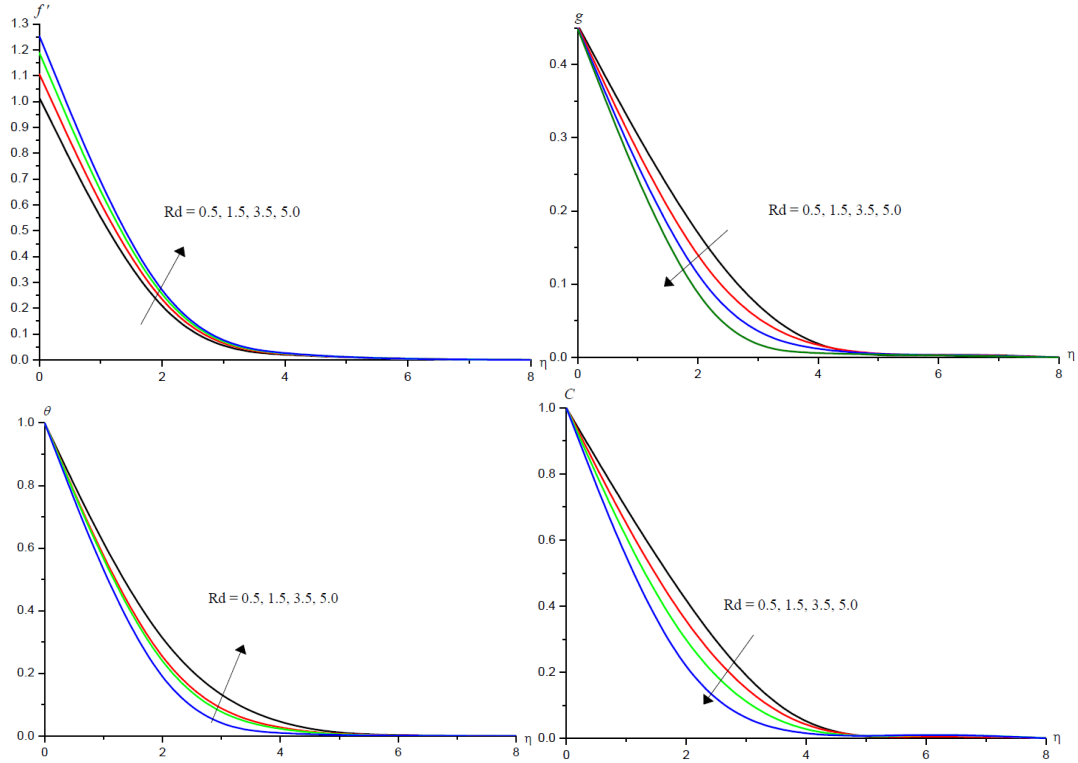

Fig.5: Variation of [a]axial velocity(f'), [b]secondary velocity(g), [c]Temperature(θ), [d]nanoconcentration(C) with Rd

G=2,M=0.5,K=0.2,Sc=0.66,γ=0.5,So=0.5,Q1=0.5,
A5=0.5,A6=0.6,A=1.05,ϕ=0.05,fw=0.2,B1=0.2,R=0.2,Pr=6.2

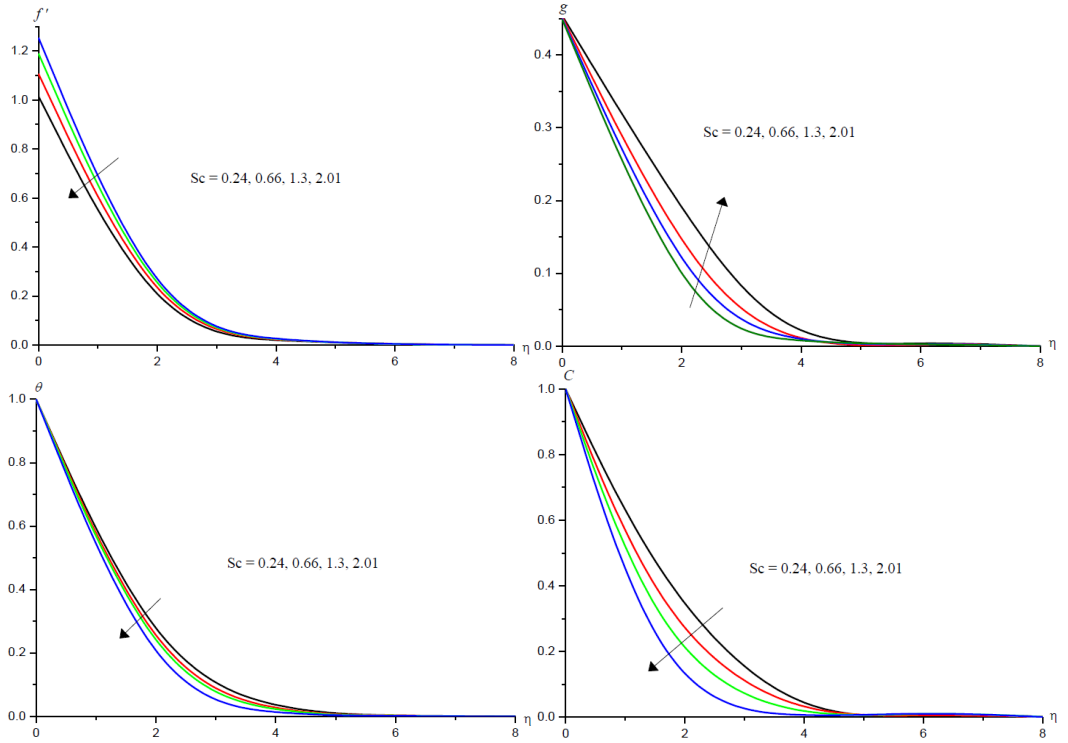

Fig.6: Variation of [a]axial velocity(f'), [b]secondary velocity(g), [c]Temperature(θ), [d]nanoconcentration(C) with Sc

G=2,M=0.5,K=0.2,Rd=0.5,γ=0.5,So=0.5,Q1=0.5,A5=0.5,
A6=0.6,A=1.05,ϕ=0.05,fw=0.2,B=0.2,R=0.2,Pr=6.2

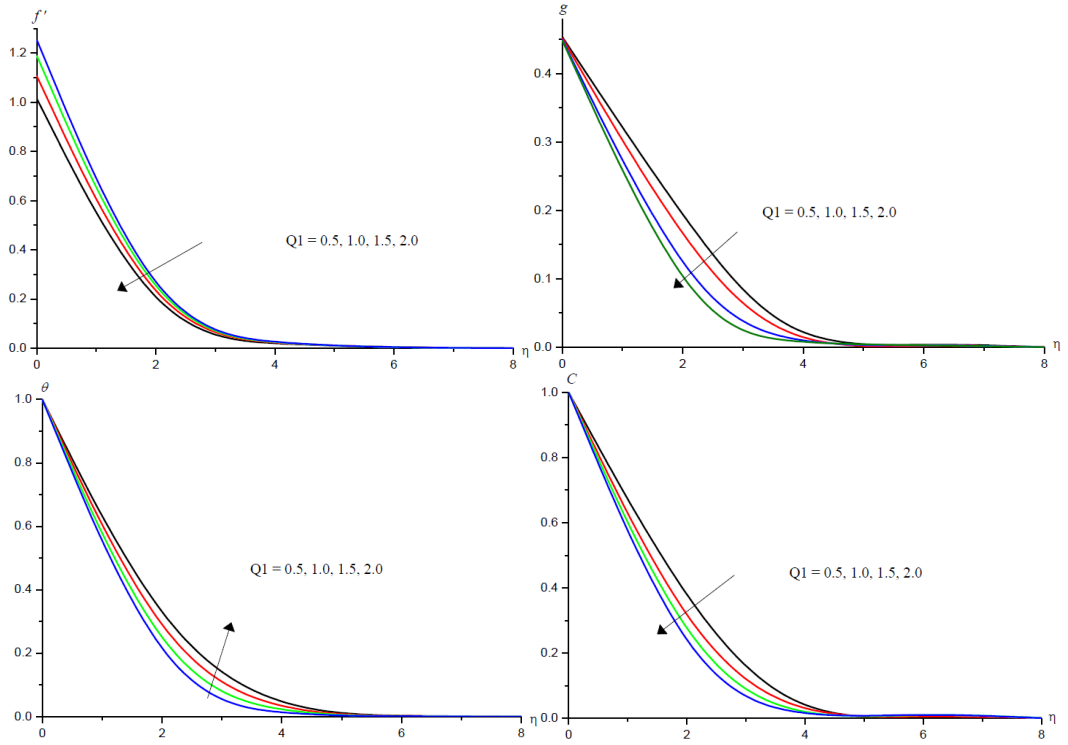

Fig.7: Variation of [a]axial velocity(f'), [b]secondary velocity(g), [c]Temperature(θ), [d]nanoconcentration(C) with Q1

G=2,M=0.5,K=0.2,Rd=0.5,Sc=0.66,γ=0.5,So=0.5,A5=0.5,
A6=0.6,A=1.05,ϕ=0.05,fw=0.2,B1=0.2,R=0.2,Pr=6.2

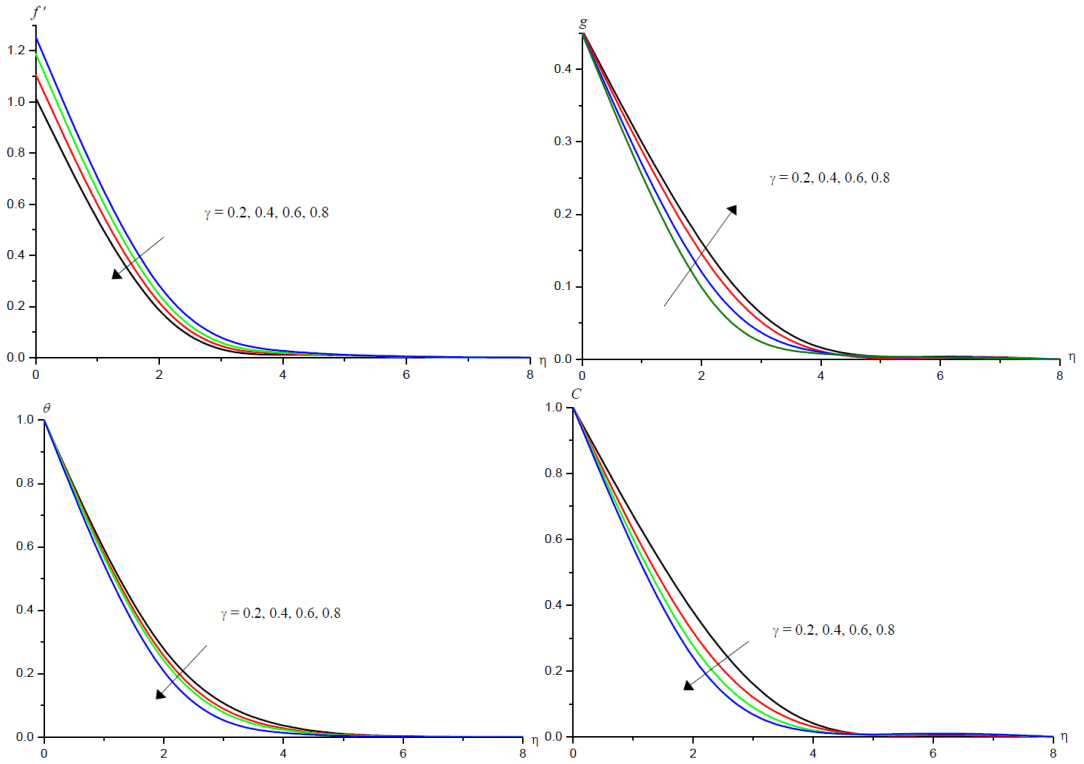

Fig.8: Variation of [a]axial velocity(f'), [b]secondary velocity(g), [c]Temperature(θ), [d]nanoconcentration(C) with γ

G=2,M=0.5,K=0.2,Rd=0.5,Sc=0.66,So=0.5,Q1=0.5,
A5=0.5,A6=0.6,A=1.05,ϕ=0.05,fw=0.2,B=0.2,R=0.2,Pr=6.2

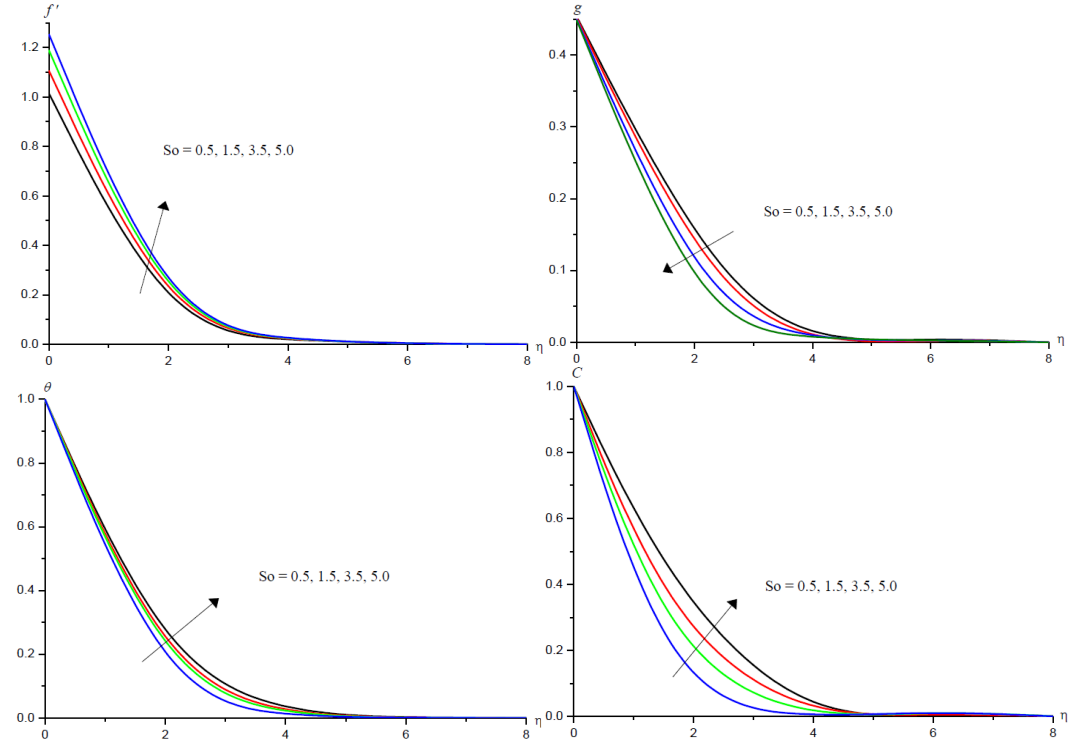

Fig.9: Variation of [a]axial velocity(f'), [b]secondary velocity(g), [c]Temperature(θ), [d]nanoconcentration(C) with S_0
G=2,M=0.5,K=0.2,Rd=0.5,Sc=0.66,γ=0.5,Q1=0.5,A5=0.5,A6=0.6,
A=1.05,ϕ=0.05,fw=0.2,B=0.2,R=0.2,Pr=6.2

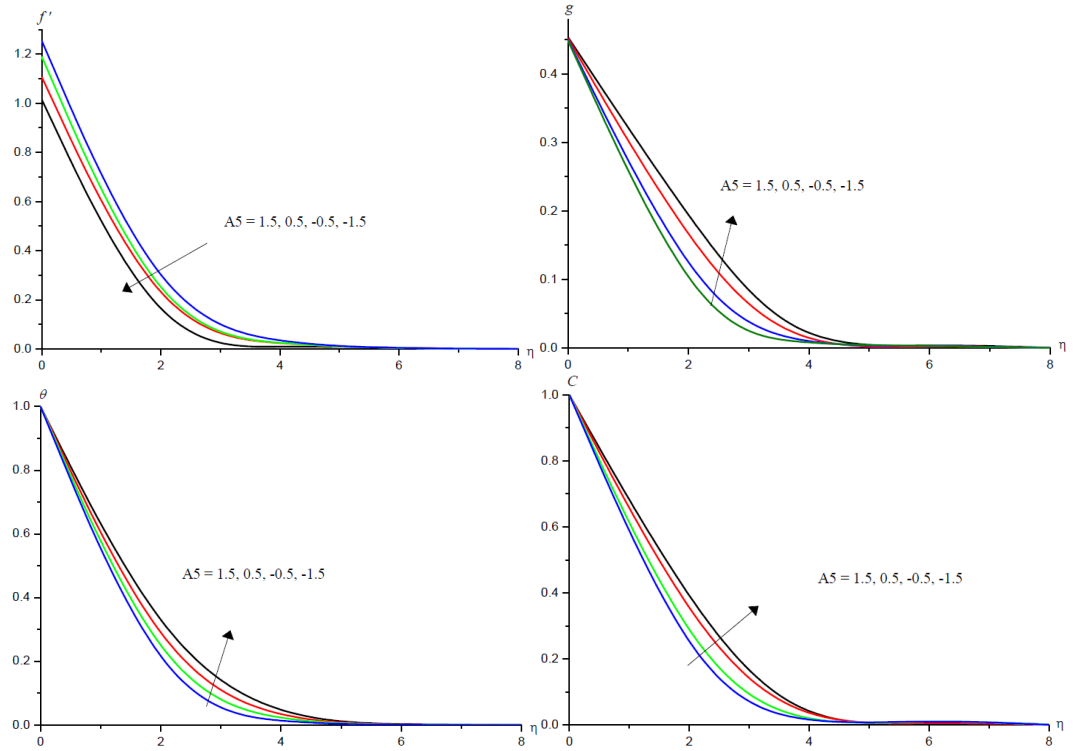

Fig.10: Variation of [a]axial velocity(f'), [b]secondary velocity(g), [c]Temperature(θ), [d]nanoconcentration(C) with A5
G=2,M=0.5,K=0.2,Rd=0.5,Sc=0.66,γ=0.5,So=0.5,Q1=0.5,A6=0.6,
A=1.05,ϕ=0.05,fw=0.2,B=0.2,R=0.2,Pr=6.2

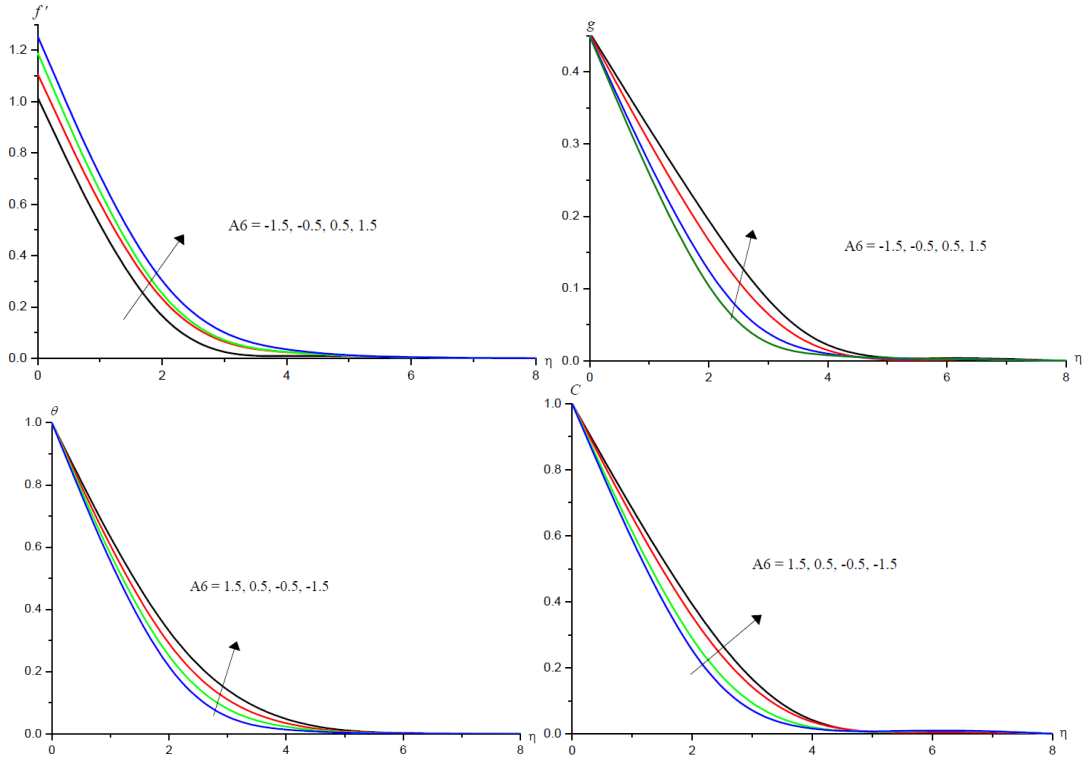

Fig.11: Variation of [a]axial velocity(f'), [b]secondary velocity(g), [c]Temperature(θ), [d]nanoconcentration(C) with A6

G=2,M=0.5,K=0.2,Rd=0.5,Sc=0.66,γ=0.5,So=0.5,Q1=0.5,A5=0.5, A=1.05,ϕ=0.05,fw=0.2,B=0.2,R=0.2,Pr=6.2

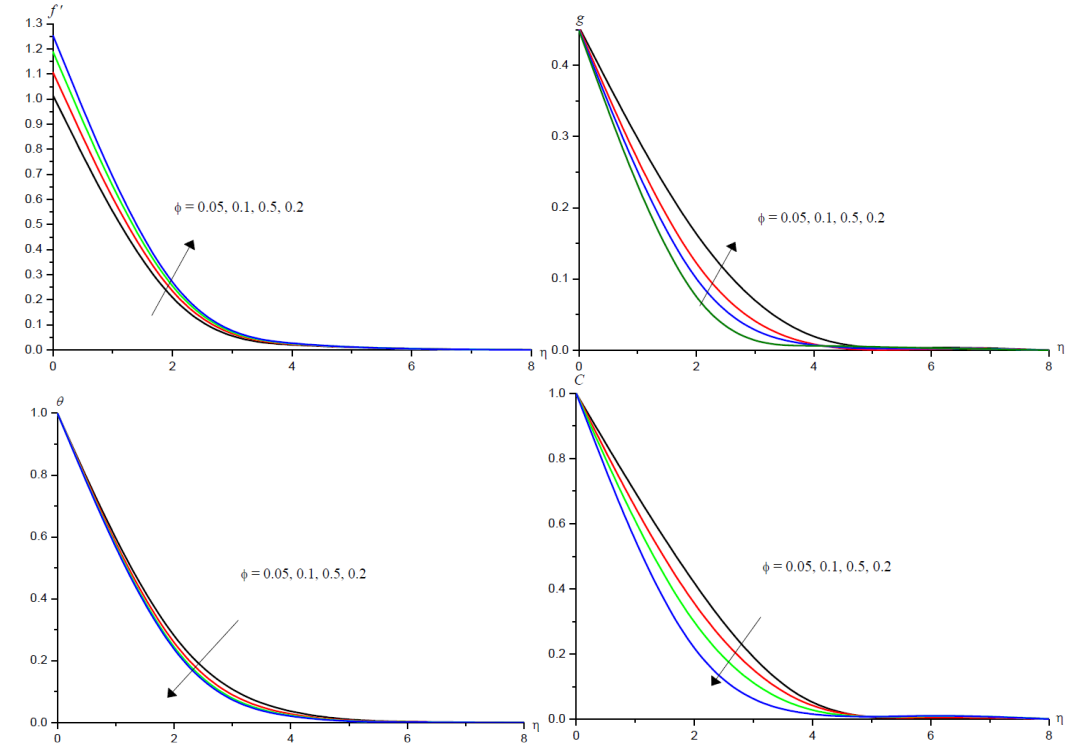

Fig.12: Variation of [a]axial velocity(f'), [b]secondary velocity(g), [c]Temperature(θ), [d]nanoconcentration(C) with ϕ

G=2,M=0.5,K=0.2,Rd=0.5,Sc=0.66,γ=0.5,So=0.5,Q1=0.5, A5=0.5,A6=0.6,A=1.05, fw=0.2,B=0.2,R=0.2,Pr=6.2

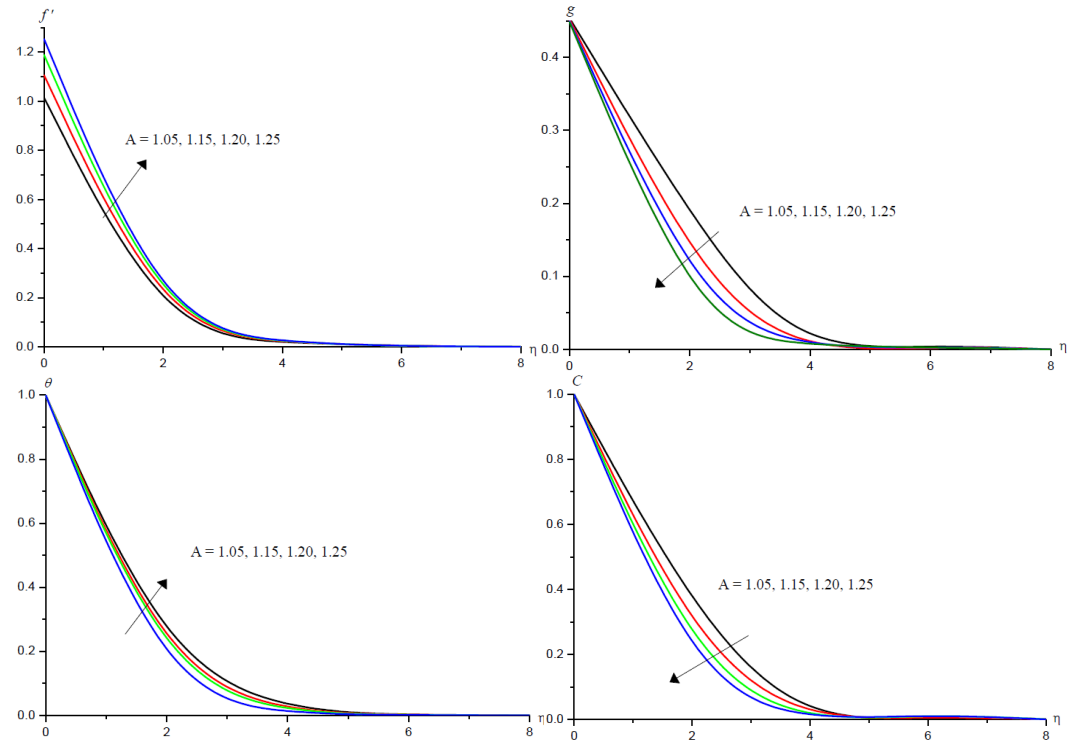

Fig.13: Variation of [a]axial velocity(f'), [b]secondary velocity(g), [c]Temperature(θ), [d]nanoconcentration(C) with A

G=2,M=0.5,K=0.2,Rd=0.5,Sc=0.66,γ=0.5,So=0.5,Q1=0.5,

A5=0.5,A6=0.6, ϕ=0.05,fw=0.2,B=0.2,R=0.2,Pr=6.2

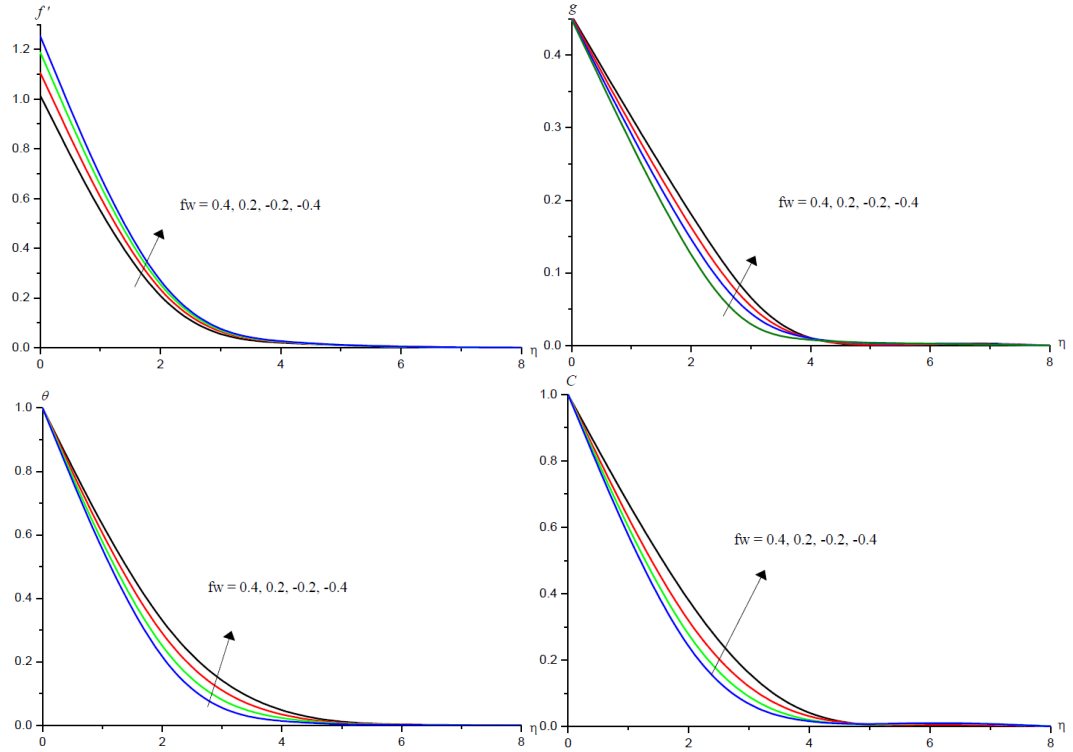

Fig.14: Variation of [a]axial velocity(f'), [b]secondary velocity(g), [c]Temperature(θ), [d]nanoconcentration(C) with fw

G=2,M=0.5,K=0.2,Rd=0.5,Sc=0.66,γ=0.5,So=0.5,Q1=0.5,

A5=0.5,A6=0.6,A=1.05,ϕ=0.05, B1=0.2,R=0.2,Pr=6.2

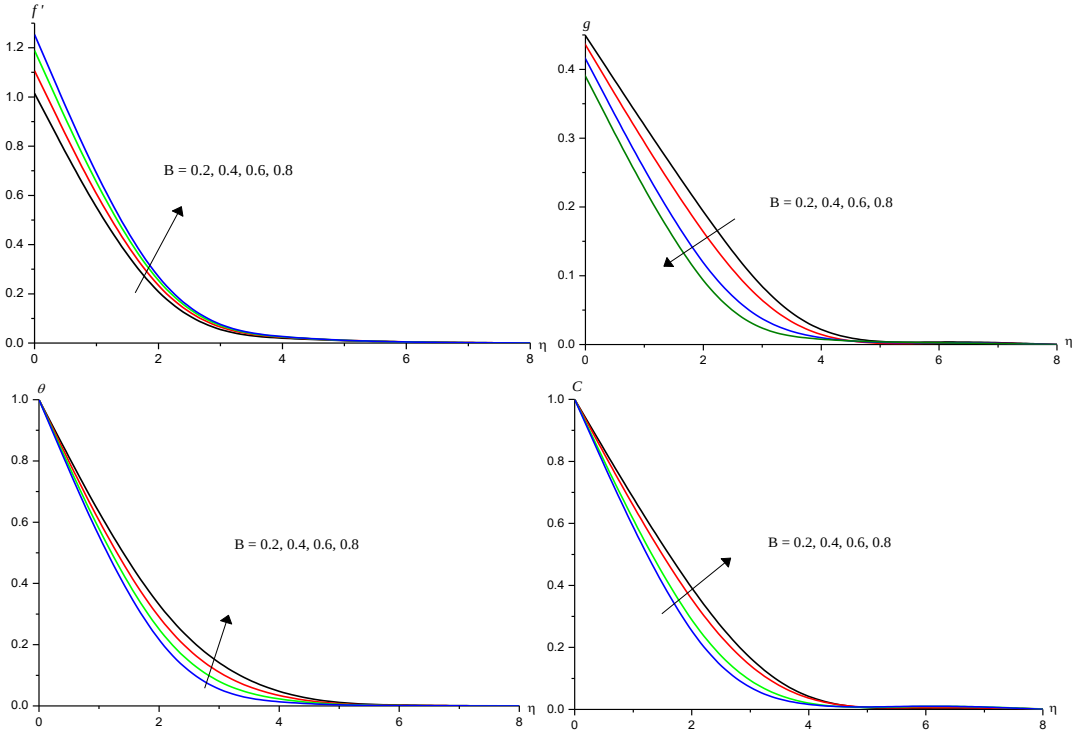

Fig.15: Variation of [a]axial velocity(f'), [b]secondary velocity(g), [c]Temperature(θ), [d]nanoconcentration(C) with B

G=2,M=0.5,K=0.2,Rd=0.5,Sc=0.66,γ=0.5,So=0.5,Q1=0.5, A5=0.5,A6=0.6,A=1.05,ϕ=0.05,fw=0.2, R=0.2,Pr=6.2

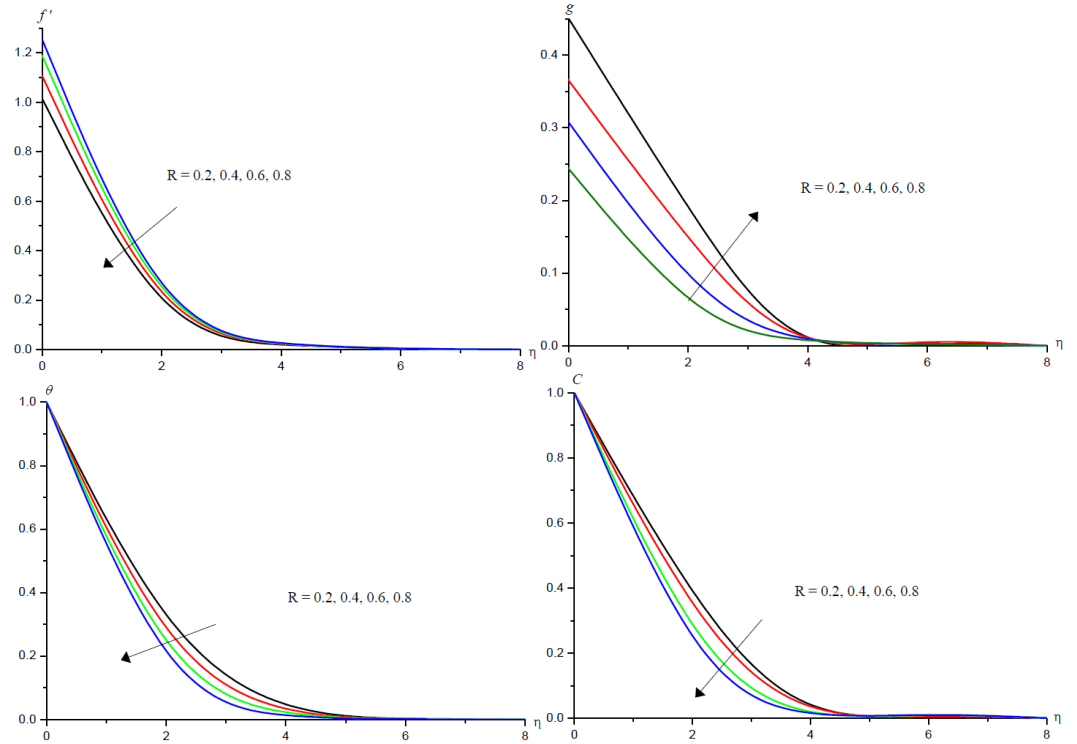

Fig.16: Variation of [a]axial velocity(f'), [b]secondary velocity(g), [c]Temperature(θ), [d]nanoconcentration(C) with R

G=2,M=0.5,K=0.2,Rd=0.5,Sc=0.66,γ=0.5,So=0.5,Q1=0.5, A5=0.5,A6=0.6,A=1.05,ϕ=0.05,fw=0.2,B=0.2,Pr=6.2

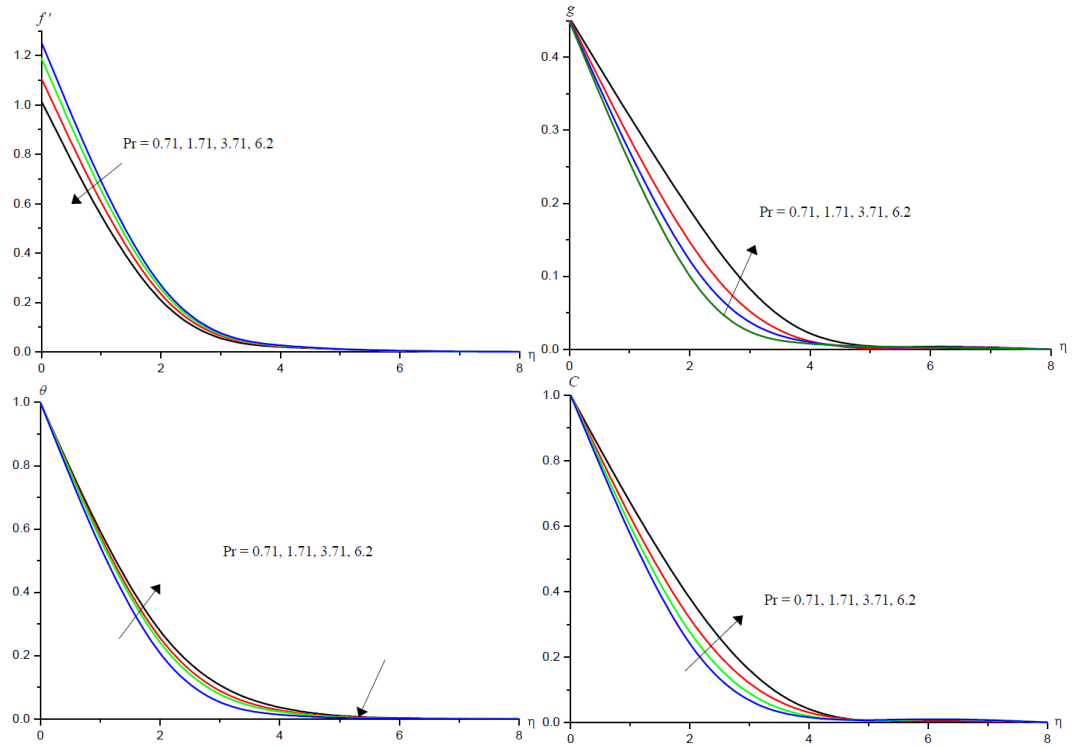

Fig.17: Variation of [a]axial velocity(f'), [b]secondary velocity(g), [c]Temperature(θ), [d]nanoconcentration(C) with Pr

G=2,M=0.5,K=0.2,Rd=0.5,Sc=0.66,γ=0.5,So=0.5,Q1=0.5,
A5=0.5,A6=0.6,A=1.05,ϕ=0.05,fw=0.2,B=0.2,R=0.2

Table 3 : Skin friction ($\tau_{x,z}$), Nusselt Number (Nu) and Sherwood Number (Sh) at $\eta=0$

Parameter		τx(0)	τz(0)	Nu(0)	Sh(0)	Parameter		τx(0)	τz(0)	Nu(0)	Sh(0)
G	2	0.148961	-0.457805	-1.16661	-0.481583	A5	0.5	0.148961	-0.457805	-1.16661	-0.481583
	4	1.0656	-0.476999	-1.24877	-0.523623		1.5	0.24084	-0.461765	-0.995071	-0.542365
	6	1.89058	-0.492251	-1.31256	-0.555485		-0.5	0.131738	-0.457054	-1.19878	-0.470073
	10	2.54547	-0.50367	-1.34633	-0.582231		-1.5	0.0185668	-0.452983	-1.33506	-0.417723
M	0.5	0.148961	-0.457805	-1.16661	-0.481583	A6	0.5	0.148961	-0.457805	-1.16661	-0.481583
	1	0.0767514	-0.488944	-1.15305	-0.4725		1.5	0.180925	-0.459016	-1.07472	-0.511357
	1.5	0.0112854	-0.516546	-1.14076	-0.464445		-0.5	0.142921	-0.457577	-1.18431	-0.475853
	2	-0.146705	-0.566663	-1.10296	-0.451323		-1.5	0.0788182	-0.455852	-1.25635	-0.449459
K	0.2	0.148961	-0.457805	-1.16661	-0.481583	ϕ	0.05	-0.135433	-0.486981	-1.11185	-0.461915
	0.4	-0.0276697	-0.532722	-1.13345	-0.459739		0.1	0.129328	-0.465244	-1.16249	-0.478356
	0.6	-0.180754	-0.594824	-1.10476	-0.441905		0.15	0.433074	-0.435998	-1.21584	-0.499697
	0.8	-0.160754	-0.574824	-1.08476	-0.421905		0.2	0.739862	-0.40217	-1.25377	-0.527794
Rd	0.5	-0.115217	-0.447444	-1.76804	-0.278719	fw	0.2	0.148961	-0.457805	-1.16661	-0.481583
	1.5	0.148961	-0.457805	-1.16661	-0.481583		0.4	-0.215845	-0.561055	-1.77165	-0.513802
	3.5	0.308616	-0.46479	-0.924636	-0.570481		-0.2	0.358702	-0.398293	-0.840704	-0.459055
	5	0.37101	-0.468691	-0.779546	-0.621464		-0.4	0.574666	-0.316688	-0.447004	-0.408887
Sc	0.24	0.149292	-0.457822	-1.16632	-0.303559	A	1.05	0.148961	-0.457805	-1.16661	-0.481583
	0.55	0.148961	-0.457805	-1.16661	-0.481583		1.15	0.221941	-0.46049	-0.972575	-0.544183
	1.3	0.148709	-0.457792	-1.16686	-0.732739		1.2	0.259414	-0.461925	-0.891561	-0.570941
	2.01	0.11287	-0.457145	-1.15226	-0.987647		1.25	0.279531	-0.462356	-0.822807	-0.590502
γ	0.2	0.148961	-0.457805	-1.16661	-0.481583	B	0.2	0.148961	-0.457805	-1.16661	-0.481583
	0.4	0.148894	-0.457802	-1.16668	-0.589819		0.4	0.112593	-0.324061	-1.14397	-0.475338
	0.6	0.148845	-0.457799	-1.16674	-0.680227		0.6	0.0904452	-0.25412	-1.13145	-0.471872
	0.8	0.11307	-0.457155	-1.15205	-0.763824		0.8	0.0651657	-0.218851	-1.10739	-0.470704
So	0.5	0.148961	-0.457805	-1.16661	-0.481583	R	0.2	0.237881	-0.121978	-1.07918	-0.457915
	1	0.149038	-0.457809	-1.16652	-0.355384		0.4	0.199554	-0.25305	-1.11656	-0.467952
	1.5	0.149269	-0.45782	-1.16626	0.0230648		0.6	0.148961	-0.457805	-1.16661	-0.481583
	2	0.113825	-0.457192	-1.15117	0.511276		0.8	0.0572502	-0.73378	-1.20894	-0.499322
Q1	0.5	0.148961	-0.457805	-1.16661	-0.481583	Pr	0.71	0.918364	-0.492321	-0.284337	-0.848796
	1	0.149302	-0.45782	-1.16602	-0.481801		1.71	0.879572	-0.490625	-0.318727	-0.822771
	1.5	0.150321	-0.457866	-1.16423	-0.482456		3.71	0.825304	-0.488226	-0.367349	-0.794939
	2	0.115882	-0.457282	-1.14709	-0.484938		6.20	0.585443	-0.478539	-0.535728	-0.716228

5. CONCLUSIONS

Three-dimensional flow, heat and mass transfer of Al_2O_3-water based nanofluid over porous stretching sheet is studied in this analysis. The velocity distributions elevated whereas temperature distributions decelerate with the higher values of (ϕ) It is worth to mention that the heat transfer rates improve as the values of ϕ increase. Increasing values of *M, R, A* and *B* decelerates the temperature of the fluid.

Higher the radiation absorption larger the primary velocity and smaller the secondary velocity in the flow region. The thickness of the thermal boundary layer grows and solutal boundary layer decays with increasing values of Q1. Both velocity profiles f' and g are enhanced, temperature and nanoconcentration reduces in based nanofluid as the nanoparticle volume fraction (ϕ) increases.

6. ACKNOWLEDGEMENT

We are thankful to the referees for their valuable suggestions for the improvement of the manuscript of the paper.

7. REFERENCES

[1]. Behseresht, A., Nogrehabadi, A. and Ghalambaz, M. (2014), "Natural-convection heat and mass transfer from a vertical cone in porous media filled with nanofluids using practical ranges of nanofluids thermo-physical properties", *Chem. Engnrg. Res. Design,* Vol. 92, pp. 447-452.

[2]. Bhargava, R., Sharma, R. and Bég, O.A. (2009), "Oscillatory chemically-reacting MHD free convection heat and mass transfer in a porous medium with Soret and Dufour effects: finite element modeling", *Int. J. Appl. Math. Mechanics,* Vol. 5, pp. 15–37.

[3]. Buongiorno, J. (2006),"Convective transport in nanofluids",*J Heat Transfer*, Vol. 128, pp. 240–250.

[4]. Chamkha, A.J., Abbasbandy, S. and Rashad, A.M.(2015), "Non-Darcy Natural Convection Flow of Non-Newtonian Nanofluid Over a Cone Saturated in a Porous Medium with Uniform Heat and Volume Fraction Fluxes", *International Journal of Numerical Methods for Heat and Fluid Flow*, Vol. 25, pp. 422-437.

[5]. Chamkha, A.J.and Abu-Nada, E. (2012), "Mixed Convection Flow in Single- and Double-Lid Driven Square Cavities Filled with Water-Al_2O_3Nanofluid: Effect of Viscosity Models", *European Journal of Mechanics - B/Fluids,* Vol. 36, pp. 82-96.

[6]. Cheng, C.Y. (2013), "Double-diffusive natural convection from a vertical cone in a porous medium saturated with a nanofluid", *J. Chinese Soc. Mech. Engrs,* Vol. 34, pp. 401-409.

[7]. Choi, S.U.S.and Eastman, J.A. (2009),"Enhancing thermal conductivities of fluids with nanoparticles", in Proceedings of the *ASME International Mechanical Engineering Congress and Exposition*, vol.66,pp. 99–105.

[8]. Dulal Pal, and Mondal, H. (2011), " Effects of Soret, Dufour, chemical reaction and thermal radiation on MHD non-Darcy unsteady mixed convective heat and mass transfer over a stretching sheet", *Commun Nonlinear SciNumerSimulat*, Vol. 16, pp. 1942–1958.

[9]. Ghalambaz, M., Behseresht, A., Behseresht, J. and Chamkha, A.J. (2015) "Effect of nanoparticle diameter and concentration on natural convection in Al_2O_3 – water nanofluids considering variable thermal conductivity around a vertical cone in porous media", *Adv. Powder Technology*, Vol. 26, pp.224 – 235.

[10]. Hayat, T., T. Muhammad, A. Alsaedi and M. S. Alhuthali, Magnetohydrodynamic three-dimensional flow of visco-elastic nanofluid in the presence of nonlinear thermal radiation, Journal of Magnetism and Magnetic Materials 385, pp.222-229 (2015).

[11]. Hayat, T.,Imtiaz, M.,Alsaedi, A. andKutbi, M.A, (2015),"MHD three-dimensional flow of nanofluid with velocity slip and nonlinear thermal radiation", *Journal of Magnetism and Magnetic Materials*, Vol. 396, pp. 31–37.

[12]. Kakac, S. andPramuanjaroenkij, A. (2009),"Review of convective heat transfer enhancement with nanofluids", *Int. J. Heat Mass Transfer,*Vol. 52,pp. 3187–3196.

[13]. Kleinstreuer, C. andFeng, Y. (2011), "Experimental and theoretical studies of nanofluid thermal conductivity enhancement: a review", *Nanoscale Res. Letters,*Vol. 6, pp. 229.

[14]. Kuznetsov, A.V. and Nield, D.A. (2010), "Natural convective boundary-layer flow of a nanofluid past a vertical plate ", *Int. J. Therm. Science,* Vol. 49 , pp. 243–247.

[15]. Kuznetstov, A.V. and Neild, D.A. (2014)"Natural convective boundary-layer flow of a nanofluid past a vertical plate: A revised model", *International journal of thermal sciences,*Vol. 77, pp. 126-129.

[16]. Liao, S. J.: On the relationship between the homotopy analysis method and Euler transform, Communications in Nonlinear Science and Numerical Simulation 15; pp.1421-1431(2010)

[17]. Madhusuadana Reddy, Y: The effect of second order slip and non-linear thermal radiation on unsteady convective heat and mass transfer flow past a stretching surface with Newtonian cooling., Journal of Xi's university of Archetecture and Technology,,V.Xii,Issue.Xii,pp.652-65(2021)

[18]. Mushtaq. A., M. Mustafa. T. Hayat and A. Alsacdi, Nonlinear radiative heat transfer in the flow of nonofluid due to solar energy. A numerical study, Journal of Taiwan Institute of Chemical Engineering, 45, pp.1176-1183 (2014).

[19]. Mustafa, M., A. Mushtaq, T. Hayat and A. Alsaedi, Model to study the non-linear radiation heat transfer in the stagnation-point ow of power-law uid, International Journal of Numerical Methods for Heat & Fluid Flow 25, (5),pp.1107-1119 (2015).

[20]. Noghrehabadi, A.,Ghalambaz, M. and Ghanbarzadeh, A. (2014), "Effects of variable viscosity and thermal conductivity on natural-convection of nanofluids past a vertical plate in porous media", *Journal of Mechanics*, Vol. 30, pp. 265-275.

[21]. Ozerinc, S., Kakac, S. and Yazıcıoglu, A. (2010),"Enhanced thermal conductivity of nanofluids: a state-of-the-art review",*Microfluid. Nanofluid,* Vol. 8 , pp. 145–170.

[22]. Pantokratores, A. and T. Fang, Sakiadis flow with nonlinear Rosseland thermal radiation, Physica Scripta, 87, (1) 015703, (2013).

[23]. Pop, I., Ghalambaz, M. and Sheremet, M. (2016),"Free convection in a square porous cavity filled with a nanofluid using thermal non equilibrium and Buongiorno models", *International Journal of Numerical Methods for Heat & Fluid Flow*, Vol. 26, pp. 671-693.

[23a] Prabavathi B, Sudarsana Reddy P, Bhuvana Vijaya R (2016): Three-dimensional Heat and Mass Transfer Flow Over a Stretching Sheet Filled with Al_2O_3-water Based Nanofluid with Heat Generation/Absorption, Journal of Nanofluids.

[24]. Puneet Rana, R. and Bhargava, (2012),"Flow and heat transfer of a Nano fluid over a nonlinearly stretching sheet: a numerical study", *Comm. Nonlinear Sci. Numer. Simulat.,* Vol. 17, pp. 212– 226.

[25]. Rashidi, M.M., Rostami, B.,Freidoonimehr, N. and Abbasbandy, S. (2014)"Free Convective Heat and Mass Transfer for MHD Fluid Flow over a Permeable Vertical Stretching Sheet in the Presence of the Radiation and Buoyancy Effects", *Ain Shams Engineering Journal*, Vol. 5,pp. 901-912.

[26]. Shehzad, S. A. ,T. Hayat, A. Alsaedi and M. A. Obid, Nonlinear thermal radiation in three-dimensional ow of Jefrey nanouid: A model for solar energy, Applied Mathematics and Computation, 248, 273-286 (2014).

[27]. Sheremet, M.A.,Oztop, H.F. and Pop, I. (2016)"MHD natural convection in an inclined wavy cavity with corner heater filled with a nanofluid", *J. Magnetism Magnetic Materials*,Vol. 416,pp. 37–47.

[28]. Sreedevi, P.,Sudarsana Reddy, P. and Chamkha, A.J. (2017) Heat and Mass transfer analysis of nanofluid over linear and non- linear stretching surface with thermal radiation and Chemical reaction, *Powder Technology,* Vol. 315,pp. 194 – 204.

[29]. Sudarsana Reddy, P. and Chamkha, A.J. (2016 a), "Soret and Dufour effects on MHD heat and mass transfer flow of a micropolar fluid with thermophoresis particle deposition", *Journal of Naval Architechure and Marine Engineering*, Vol. 13,pp. 39-50.

[30]. Sudarsana Reddy, P. and Chamkha, A.J. (2016 b), "Soret and Dufour Effects on unsteady MHD heat and mass transfer over a stretching sheet with thermophoresis and non-uniform heat generation/absorption", *Journal of Applied Fluid Mechanics,* Vol. 9,pp. 2443-2455.

[31]. Sudarsana Reddy, P. and Chamkha, A.J. (2016 c),"Soret and Dufour effects on MHD convective flow of Al_2O_3–water and TiO_2–water nanofluids past a stretching sheet in porous media with heat generation/absorption", *Advanced Powder Technology*, Vol. 27 pp. 1207-1218.

[32]. Sudarsana Reddy, P., Sreedevi, P. and Chamkha, A.J. (2017) "MHD boundary layer flow, heat and mass transfer analysis over a rotating disk through porous medium saturated by Cu-water and Ag-water nanofluid with chemical reaction", *Powder Technology*, Vol. 307, pp. 46–55.

[33]. Sundar, L.S., Sharma,K.V., Naik, M.T. and Singh, M.K. (2013), "Empirical and theoretical correlations on viscosity of nanofluids: a review ", *Renew. Sustain. Energy Rev* , Vol. 25, pp.670–686.

[34]. Tasawar Hayat,Maria Imtiaz,Ahmad alsaedi and Marwan A.Kuthi:MHD three-dimensional flow of nanofluid with velocity slip and n0nlinear thermal radiation,

Journal of Magnetism and Magnetic Materials., http://dx.doi.org/10.1016/j.jmmm,(2015)

[35]. Dr. Gnanaprasunamba K. (2022), "Effect of brownian motion and thermophoresis on nanofluid past a stretching surface with variable viscosity and newtonian cooling inspired by thermal radiation, ymer || issn : 0044-0477 volume 21 : issue 4 (April) - 2022., http://ymerdigital.com/current-issue/